J Neuropathol Exp Neurol
Vol. 66, No. 12
December 2007
pp. 1100–1117
Copyright © 2007 by the American Association of Neuropathologists, Inc.

ORIGINAL ARTICLE

A Novel Cerebral Microangiopathy With Endothelial Cell Atypia and Multifocal White Matter Lesions: A Direct Mycoplasmal Infection?

Gabriele M. Zu-Rhein, MD, Shyh-Ching Lo, MD, PhD, Christine M. Hulette, MD, and James M. Powers, MD

Abstract

We present 3 sporadic cases of a subacute to chronic, progressive motor (i.e. weakness, ataxia, spasticity, dysarthria, and dysphagia) and cognitive disorder in adults of both sexes, without proven immunocompromise or malignancy. Neuroimaging studies revealed tiny calcifications with atrophy of the cerebrum, pons, and midbrain in 1 patient, cerebral atrophy in another, and cerebral atrophy and periventricular white matter hyperintensities in the third. Clinical diagnoses included cortico-pontine-cerebellar degeneration, mixed neurodegenerative disorder, progressive supranuclear palsy, diffuse Lewy body disease, and Lyme disease. One atrophic brain revealed widely disseminated, millimeter-sized gray lesions in cerebral white matter and obscured anatomic markings of the basis pontis. The most conspicuous microscopic feature in all was capillaries with focally piled up endothelial nuclei, some of which appeared to be multinucleated, or enlarged, hyperchromatic crescentic single nuclei. Although seen mostly without associated damage, they were also noted with white matter lesions displaying vacuolation, demyelination, spheroids, necrosis, vascular fibrosis, and mineralization; these were most severe in the basis pontis. Immunostains and probes to herpes simplex virus-I, -II, and -8; adenovirus, cytomegalovirus, varicella-zoster, Epstein-Barr virus, measles, JC virus, and herpes hominis virus-6 were negative. Electron microscopy revealed no virions in endothelial cells with multilobed or multiple nuclei and duplicated basal laminae. However, mycoplasma-like bodies, mostly 400 to 600 nm in size, were found in endothelial cell cytoplasm and capillary lumina. Platelets adhered to affected endothelial cells. Polymerase chain reaction and immunohistochemistry of fixed samples for *Mycoplasma fermentans* were negative; other species of *Mycoplasma* remain viable pathogenic candidates.

Key Words: Blood-brain barrier, Brain endothelium, *Mycoplasma,* Myelinated axon, Ultrastructure, Immunohistochemistry, Virus.

INTRODUCTION

The pathogenetic association between *Mycoplasmas,* parasitic, epicellular, or intracellular bacteria lacking a cell wall and CNS disease has been controversial and perhaps under-reported, in part because culture isolation of the microbes from either cerebrospinal fluid (CSF) or CNS tissue samples is protracted and difficult. Moreover, the absence of a cell wall prevents their recognition by the traditional bacterial Gram stain. More modern molecular techniques, especially the polymerase chain reaction (PCR), are more sensitive but less specific for detecting viable organisms. Despite these limitations, a spectrum of CNS lesions (e.g. meningitis, meningoencephalitis, encephalitis, transverse myelitis, brain abscess, and even infarction) has been reported. The most common *Mycoplasma* species reported in such neurologic situations is *Mycoplasma pneumoniae,* usually present in the setting of an atypical pneumonic process; but it still is a rare complication (i.e. less than 0.1% of all *M. pneumoniae* infections), which is more common in children than adults. Early-onset encephalitis (less than 7 days after the onset of fever) is believed to be due to direct invasion of CSF or brain tissue, perhaps by the hematogenous route. Late-onset encephalitis (greater than 7 days after the onset of fever) is thought to be more likely related to a hypercoagulable state or immune-mediated injury leading to acute disseminated encephalomyelitis or vasculitis. The latter pathogenic mechanism, particularly acute disseminated encephalomyelitis, has been the most favored. Neuropathologic confirmation of cases of suspected direct invasion or infection has been wanting (reviewed in References 1–5).

Over a span of 14 years, we have encountered a progressive and fatal subacute to chronic neurologic syndrome in 3 immunocompetent adults. At autopsy all 3 patients displayed correlative neuropathologic lesions that we believe are unique and reflect the recognition of a new

From the Department of Pathology (GMZ-R), University of Wisconsin Medical School, Madison, Wisconsin; Department of Infectious and Parasitic Diseases and Pathology (SC-L), Armed Forces Institute of Pathology, Washington, DC; Department of Pathology (CMH), Duke University Medical Center, Durham, North Carolina; and Departments of Pathology and Neurology (JMP), University of Rochester Medical Center, Rochester, New York.

Send correspondence and reprint requests to: James M. Powers, MD, University of Rochester Medical Center, Department of Pathology, Box 626, 601 Elmwood Avenue, Rochester, NY 14642; E-mail: james_powers@urmc.Rochester.edu

This work was supported in part by U.S. Public Health Service National Institute on Aging Grants P50 AGO5128 and P30 AGO28377 and was awarded an Honorable Mention for the Moore Award at the 2007 American Association of Neuropathologists meeting in Washington, D.C.

Downloaded from http://jnen.oxfordjournals.org/ by guest on June 7, 2016

Copyright © 2007 by the American Association of Neuropathologists, Inc. Unauthorized reproduction of this article is prohibited.

CNS disease. Furthermore, we present ultrastructural evidence to suggest that this novel disease could result from a direct infection of brain endothelial cells by an unidentified *Mycoplasma* species of microbes.

MATERIALS AND METHODS

Clinical Summaries

The first patient, a woman from Wisconsin, was 56 years old at the time of her death in 1990. She had primary hypothyroidism since 1963. The neurologic history apparently began with recurrent right hemicranial headaches in 1979 with pain over the right eye, ptosis of the right eyelid, and twitching of the left face. In 1982 she complained of a transient deficit in her right visual field, periorbital headache, numbness of the right hand, and slurred speech. Results of a computerized tomographic (CT) scan were essentially unremarkable, except for some "slight brain atrophy." Both episodes were believed to be complications of migraine. During 1985 to 1987 she developed a progressive gait disturbance with stiffness of her legs, leg weakness, and ataxia. In 1987 she was noted to have clumsiness, postural tremor, hyperreflexia, and dysarthria. A CT scan showed atrophy of the cerebral and cerebellar cortices, the specific nature of which was unknown. In 1988 she was noted to have spastic paraparesis and she complained of trouble swallowing. A magnetic resonance imaging (MRI) study revealed atrophy of both cerebral hemispheres, a small pons and midbrain, and atrophy of the superior vermis. During the next 2 years she became progressively more spastic-ataxic and developed a neurogenic bladder. She also developed some cognitive dysfunction and emotional lability. In March 1990 she was admitted with acute weakness of her left arm and leg and left gaze paresis. Her CSF showed slightly increased protein but was acellular and aseptic. An electroencephalogram revealed generalized slowing, and CT scans showed numerous tiny calcific densities throughout the brain parenchyma. She became comatose and died in 1990. No significant past or family histories were noted to elucidate the nature of her neurologic illness, except that her mother also had a thyroid problem. She had a complete autopsy. Significant systemic findings consisted only of an absent thyroid gland. There were no atypical findings in the endothelial cells of any systemic organ. The referring pathologist's diagnosis was progressive multifocal leukoencephalopathy.

The second patient, a man from South Carolina, was 41 years old at the time of his death in 1993. At age 39 progressive lateral sclerosis was diagnosed because of a problem with running that started at about age 37. He interpreted this problem as being more related to balance than to muscle weakness; he also had some speech difficulty. On examination he was found to have generalized spasticity including spasticity of the bulbar musculature. These problems progressed until he was confined to a wheelchair and he subsequently developed dementia and irritability. An MRI scan in 1992 showed some brain atrophy. He sustained a generalized tonic seizure in 1992. Repeat MRI confirmed the generalized atrophy, as well as an arachnoid cyst in the left temporal area. At that time his EEG was normal. He had a severe episode of status epilepticus that resulted in marked hypoxic damage. Seizures continued to be a problem and he subsequently developed a dense left-sided hemiparesis. In 1993, an EEG showed slowing on the left side and seizure activity in the left occipital area. He had a brain-only autopsy. The original diagnosis was primary myelinopathy.

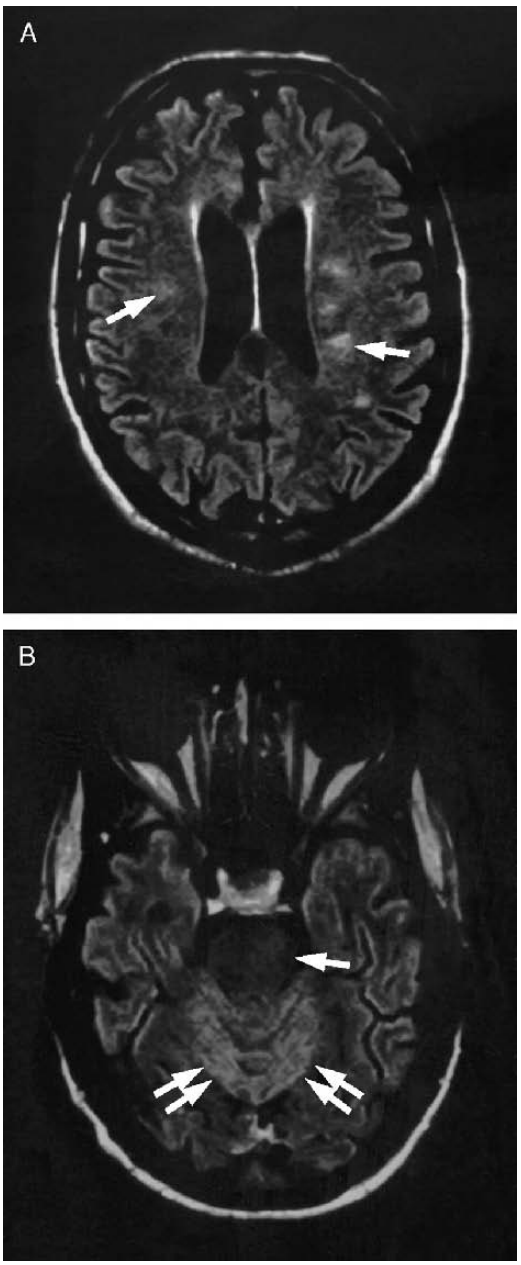

FIGURE 1. **(A)** Patient 3. Fluid-attenuated inversion recovery (FLAIR) image illustrating non-specific bilateral, but asymmetric, high-intensity abnormalities (arrows) of cerebral white matter. **(B)** Patient 3. FLAIR image showing an equivocal lesion in the left basis pontis (arrow) and slightly increased signal of the entire cerebellar cortex (double arrows). Patient 3.

Downloaded from http://jnen.oxfordjournals.org/ by guest on June 7, 2016

© 2007 American Association of Neuropathologists, Inc.

Copyright © 2007 by the American Association of Neuropathologists, Inc. Unauthorized reproduction of this article is prohibited.

TABLE. Immunohistochemistry

Antibody	Vendor	Species	Dilution	Retrieval
Adenovirus	Chemicon, Temecula, CA	Mouse monoclonal	1:50, 5 minutes	Proteinase K, 5 minutes
CMV	DAKO, Carpenteria, CA	Mouse monoclonal	1:100	Proteinase K, 5 minutes
HHV-6B	Chemicon	Mouse monoclonal	1:200	Citrate pH 6
HSV-1-2	DAKO	Rabbit polyclonal	1:3000, prediluted	Citrate pH 6
HSV-8	Yuan Chang, MD	Mouse monoclonal	1:1000	None
JCV (SV40)	Santa Cruz Biotechnology; Santa Cruz, CA	Rabbit polyclonal	1:400	Citrate pH 6, 30 minutes
Measles	Chemicon	Mouse monoclonal	1:10,000	None
V-Z	Biogenesis; Poole, England	Mouse monoclonal	1:50	Proteinase K, 4 minutes
IL-1α	Genzyme; Cambridge, MA	Rabbit polyclonal	1:300	None
TNF-α	Santa Cruz	Mouse monoclonal	1:5	None
CD31	DAKO	Mouse monoclonal	1:25	Citrate pH 6
CD34	DAKO	Mouse monoclonal	1:75	Citrate pH6
Factor VIII	DAKO	Mouse monoclonal	1:75	Proteinase K, 4 minutes
Fibrin	DAKO	Mouse monoclonal	1:12K	Proteinase K, 3 minutes
p53	DAKO	Mouse monoclonal	1:75	Citrate pH 6
Ki-67	DAKO	Mouse monoclonal	1:100	Citrate pH 6 and pH 9.9

All DAKO virus, adenovirus, and V-Z immunohistochemical stains were done in a DAKO Autostainer using the DAKO Retrieval System (citrate buffer at pH 6), unless otherwise specified. HHV-6B (p101), HSV-8, measles, IL-1α, and TNF-α stains were performed by hand. All stains were performed using appropriate positive and negative (i.e. primary antibody omitted) controls.

CMV, cytomegalovirus; HHV, herpes hominis virus; HSV, herpes simplex virus; JCV, JC virus; SV40, Simian virus 40; V-Z, varicella-zoster; IL-1α, interleukin-1α; TNF-α, tumor necrosis factor-α.

The third patient, a man from Georgia, was 67 years old at the time of his death in 2004. He had a history of progressive weakness and difficulty walking for about 3 years. Historically, there existed the possibility of a tick bite in August of 2001, after which he experienced pain in his knees and fatigue. The initial serology for Lyme disease was negative. In 2002 he experienced an episode of word recall difficulty that was interpreted as a possible transient ischemia attack. In 2002, he also developed progressive difficulty in walking, slowed responses, sleeping difficulties, and a very low voice. The leading clinical differentials included Lewy body dementia and normal pressure hydrocephalus. Results of a CT scan without contrast and CSF examinations were normal. MRI (T1-weighted, fluid-attenuated inversion recovery [FLAIR], T2-weighted, and diffusion images) without contrast revealed only mild cerebral atrophy. Two months later and in another institution, an MRI study with contrast also revealed "minor periventricular white matter changes noted related to ischemia". Three months later, results of a positron emission tomographic brain scan were unremarkable. In 2003 he was found to have a positive antigen in his urine for Lyme disease, interpreted as a false positive. In 2003 he was still weak and had more trouble walking. At that time results of a test for Epstein-Barr virus were positive, but Lyme disease was still considered a possibility, for which he was treated with zithramycin (Zithromax) and Augmentin XR for 5 weeks. In October, results of another MRI study (FLAIR) confirmed the hyperintensities in the periventricular white matter (Fig. 1A), particularly on the left, which had progressed since the last MRI. No areas of abnormal enhancement were noted. Additionally, the FLAIR sequences showed a focal high signal abnormality in the left basis pontis and diffuse high signal change in the cerebellar cortex, as well as a milder change in cerebral cortex (Fig. 1B). In early 2004, an alternate diagnosis of progressive supranuclear palsy had been entertained, but Lyme disease was still considered. He was then treated with Minocin, Zithromax, Plaquenil, Levaquin and Rocephin without success. In June 2004, upon awakening, he was hardly able to speak or to move. He died 2 months later. A complete autopsy was performed. Significant systemic findings included suppurative lobular pneumonia caused by aspirations, emphysema and interstitial fibrosis, subclinical giant cell (syncytial) hepatitis, and an abdominal atherosclerotic aneurysm. No systemic endothelial cell lesions were noted, but he did display some hepatic syncytia (giant cell change) and mild fibrosis, suggestive of a subclinical hepatitic process. Of note, a PCR evaluation of a piece of brain (Medical Diagnostic Laboratories L.L.C., Hamilton, NJ) failed to reveal any evidence of *Borrelia burgdorferi*. The referring pathologist's diagnosis was idiopathic multifocal necrotizing leukoencephalopathy.

Neuropathologic Methods

Formalin-fixed, paraffin-embedded sections from all levels of the neuraxis were initially stained with hematoxylin and eosin. Subsequently, a variety of traditional myelin, axon, neuronal, connective tissue, and bacterial stains was performed.

Immunohistochemical Methods and Polymerase Chain Reaction

Because viruses, particularly TR 1.3 murine leukemia virus, can produce endothelial cell lesions similar to those in our 3 patients (6), 2 cerebral samples of patient 3 were

© 2007 American Association of Neuropathologists, Inc.

Downloaded from http://jnen.oxfordjournals.org/ by guest on June 7, 2016

Copyright © 2007 by the American Association of Neuropathologists, Inc. Unauthorized reproduction of this article is prohibited.

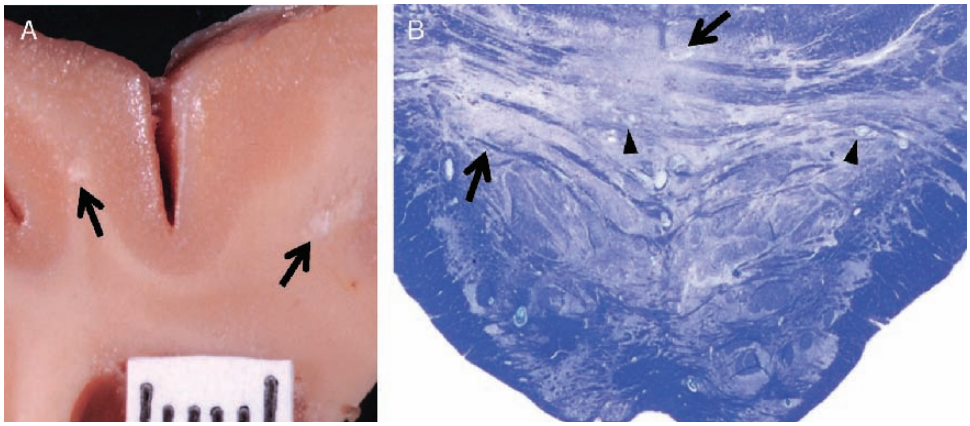

FIGURE 2. **(A)** Coronal section of frontal lobe displaying 2 white foci (arrows) of mineralization. Scale in millimeters. Patient 1. **(B)** Transverse section of pons exhibiting multiple large (arrows) and small punctate (arrowheads) areas of decreased myelin staining, particularly of the crossing fibers. Luxol fast blue; original magnification: 2×. Patient 1.

immunostained with commercial antibodies to adenovirus, herpes simplex virus-1 and -2, varicella-zoster, JC virus, measles and herpes hominis virus-6, whereas 4 cerebral samples of patient 3 were immunostained with a commercial antibody to cytomegalovirus (Table), and treated with an EBER probe for Epstein-Barr virus (prediluted, proteinase K for 12 minutes; Ventana, Tucson, AZ). The same 2 cerebral samples of patient 3 were immunostained for herpes simplex virus-8 antigen using an antibody (1:1000 without retrieval), along with a Kaposi sarcoma positive control, generously supplied by Dr. Yuan Chang (University of Pittsburgh). Finally, the same 2 cerebral samples of patient 3 were immunostained for an Epstein-Barr virus membrane protein and probed for Epstein-Barr virus (EBER) by Dr. Clayton Wiley (University of Pittsburgh). In view of the ultrastructural findings (see Results), other cerebral samples from patients 1 and 3 were immunostained with 3 monoclonal antibodies (G2, C19, and C21) developed against different *M. fermentans* membrane proteins. Also, 10-μm sections (5 sections per PCR reaction tube) were cut for a PCR study. Three different methods (phenol/chloroform, DNAzol, and QIAamp Tissue Kit) were used to examine DNA extractions of the formalin-fixed, paraffin-embedded tissue samples. Formalin-fixed, paraffin-embedded cell pellets of cultured *M. fermentans* and 2 blocks from a case with no evidence of mycoplasmal infection were processed in parallel as the positive and negative controls, respectively. Details of PCR testing for *M. fermentans* were described previously (7).

To further characterize the endothelial cell lesions, antibodies to factor VIII, CD31, CD34, tumor necrosis factor (TNF)-α, interleukin (IL)-1α, p53, Ki-67, and fibrin (Table) were applied to cerebral and cerebellar sections from all 3 patients, as well as a pontine section from patient 3; a reticulin stain was performed on the same sections. To further characterize the white matter lesions, sections from each patient were immunostained for amyloid precursor protein (rabbit polyclonal, 1:10,000, citrate pH 6; Chemicon) and stained for calcium (alizarin red) and iron (Perl's Prussian Blue).

Electron Microscopic Methods

Patient 1

Samples were selected from the molecular and granular layers of the cerebellar cortex after they had been fixed in buffered formalin for 11 months. They were fixed in 2.5% glutaraldehyde-2% paraformaldehyde solution (Karnovsky), rinsed in phosphate buffer solution, postfixed in 2% osmium tetroxide, dehydrated in graded alcohols, and embedded in Epon/Araldite. Sections were contrasted with lead citrate and uranyl acetate and were viewed in a JOEL 100 CX electron microscope. Eighty pictures were obtained from 5 blocks. Also, samples were fixed in 2% glutaraldehyde, postfixed in 2% osmium tetroxide, and embedded in Epon 812. Sections were contrasted with lead citrate and uranyl acetate and viewed in a Philips 300 electron microscope. Ninety pictures were obtained from 4 blocks.

Patient 2

Samples were selected from the cerebellar cortex after they had been fixed in buffered formalin for 12.5 years. They were fixed in 2% glutaraldehyde, postfixed in 2% osmium tetroxide, and embedded in Epon 812. Sections were contrasted with lead citrate and uranyl acetate and viewed in a Philips 300 electron microscope. Twenty-six pictures were obtained from 2 blocks.

Patient 3

Samples were selected from cerebellum, parietal and occipital cortex and subcortex, and basal ganglia after they had been embedded in paraffin for about 2.3 years. They were deparaffinized, fixed in 2.5% glutaraldehyde, postfixed in 2% osmium tetroxide, and embedded in Epon 812. Sections were stained with lead citrate and uranyl acetate and viewed in a Philips 300 or a Hitachi 7000 electron microscope. Forty-three pictures were obtained from 9 blocks. In addition, part of a stained paraffin section of a white matter lesion with atypical capillary endothelium was obtained by the "pop-off" method and processed for electron

© 2007 American Association of Neuropathologists, Inc.

Downloaded from http://jnen.oxfordjournals.org/ by guest on June 7, 2016

Copyright © 2007 by the American Association of Neuropathologists, Inc. Unauthorized reproduction of this article is prohibited.

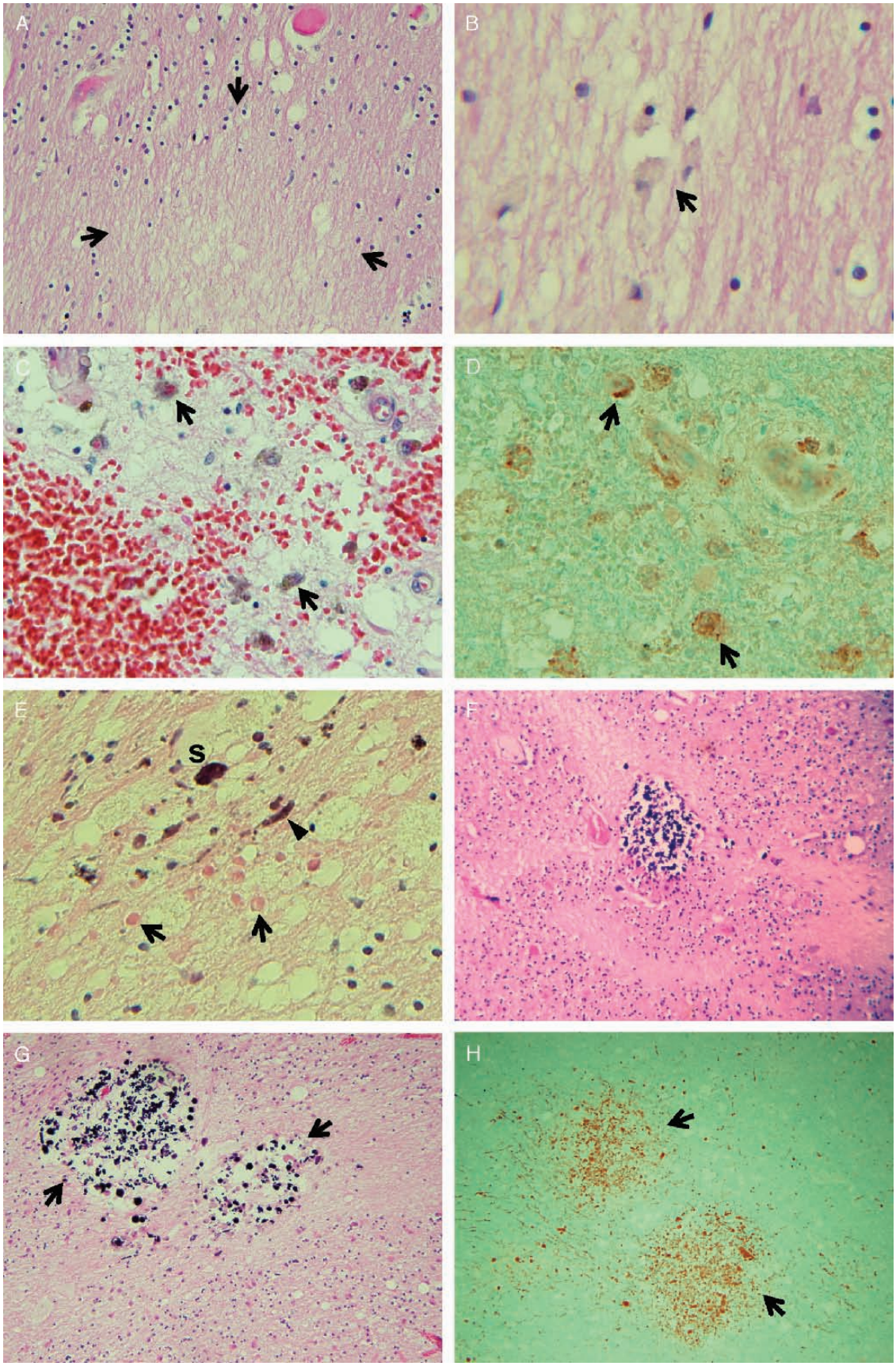

© 2007 American Association of Neuropathologists, Inc.

Downloaded from http://jnen.oxfordjournals.org/ by guest on June 7, 2016

Copyright © 2007 by the American Association of Neuropathologists, Inc. Unauthorized reproduction of this article is prohibited.

microscopy according to instructions (8). No serial ultrathin sections were obtained for any of the 3 cases.

Control Cases

Two age-matched autopsy cases (a 54-year-old woman and a 69-year-old man) were selected as procedural controls for the deparaffinized specimens. Review of sections from 2 Epon blocks of cerebellar tissue revealed some chromatin loss of nuclei as the only abnormality of capillaries.

Disease Controls

Some white matter lesions in these patients were similar or identical to those reported as multifocal necrotizing leukoencephalopathy (MNL) with pontine predilection in immunosuppressed patients (9), whereas others resembled those of osmotic myelinolysis/central pontine myelinolysis (10). Consequently, we examined representative hematoxylin and eosin-stained slides from these diseases, as well as a few others, for endothelial cell abnormalities: 7 cases of MNL (28–73 years; 4 men and 3 women) in immunocompromised patients; 3 cases of MNL in apparently immunocompetent patients (61–85 years; 1 man and 2 women); 3 cases of toxic leukoencephalopathy (46–56 years; 2 men and 1 woman); 4 cases of osmotic myelinolysis in cerebral white matter or pons (22–85 years; 3 men and 1 woman); and 1 case of bacterial sepsis (50 years; woman).

RESULTS

Neuropathologic Findings

Gross Findings

The brain of patient 1 had a fixed weight of 980 g. There was marked atrophy of the frontal gyri with widening of the sulci, cloudy leptomeninges, and compensatory ventriculomegaly. The pons and medullary pyramids were atrophic, and the anatomical markings of the basis pontis were obscured. The globus pallidus displayed an orange discoloration bilaterally. The cerebellum was normal. Of note, there were numerous millimeter-sized, ill-defined gray lesions in the pons and cerebral white matter, particularly subcortical; some had yellow centers (Fig. 2A).

The brain of patient 2 had a fixed weight of 820 g. The meninges were tinged with blood, particularly over the parietal gyri. Marked atrophy of the cerebral cortex and subcortical nuclei, right greater than left, and particularly of the right occipital cortex was observed. The cerebellum was less atrophic, left more than right. There also was slight pallor of the substantia nigra, moderate atrophy of the cerebral peduncles and pons, and a right temporal infarct that involved the hippocampus. Of note, the cerebral white matter had a granular appearance, right greater than left.

The brain of patient 3 had a fresh weight of 1,250 g. No gross abnormalities were seen, except for some mild ventricular dilatation.

Light Microscopic Findings

Only the light microscopic features common to all 3 patients will be described in detail here. The essential light microscopic lesions, which we believe are unique, are a combination of 1) multifocal lesions in white matter at all levels of the neuraxis and 2) endothelial cell abnormalities of both gray and white matter, the latter often in proximity to, or rarely within, the white matter lesions.

The white matter lesions are usually small (mm to 1 cm) and multiple; they are seen primarily in cerebral hemispheric white matter and basis pontis (Fig. 2B), but to a lesser degree at all levels of the neuraxis. However, only the upper cervical cord was available in patients 1 and 2, and no spinal cord was sampled in patient 3. The lesions often have a linear or reticular outline. They are highly variable in the degree of myelin and axonal damage. In some, there is only anuclear pallor (Fig. 3A), reflecting a loss of oligodendrocytes and perhaps some intramyelinic or vasogenic edema. In others there is vacuolation, tissue rarefaction, and a variable, but usually mild, infiltration of lipophages (Fig. 3B). Myelin abnormalities are confirmed by a reduction or loss of myelin staining with Luxol fast blue (Fig. 2B). Some macrophages are weakly periodic acid-Schiff- or Luxol fast blue-positive. Siderophages are infrequent, and fresh petechial hemorrhages are rare in the lesions (Fig. 3C). Macrophages also labeled with antibodies to CD-68 and TNF (Fig. 3D), but not to IL-1α, particularly in patient 3. With the exception of such sparse macrophages, inflammatory cells (e.g. lymphocytes) are conspicuously absent. Reactive astrocytes in white matter and some endothelial cells also express TNF, but less intensely than macrophages. Axonal sparing is seen in early myelin lesions, whereas severe to total axonal loss is evident in advanced lesions with silver stains. Axonal swellings and spheroids are also common in the latter; some axons and spheroids are mineralized (Fig. 3E). Some millimeter-sized areas of dystrophic calcification can be seen in the center of these

FIGURE 3. **(A)** Focus of myelin pallor, loss of oligodendrocytes, and rarefaction in cerebral white matter (arrows). Hematoxylin and eosin (H and E); original magnification: 200×. Patient 1. **(B)** A focus of myelin pallor in cerebral white matter with a few macrophages (arrow). H and E; original magnification: 600×. Patient 1. **(C)** A focus of cerebral white matter damage containing a few siderophages (arrows) and rare fresh hemorrhage. H and E; original magnification: 400×. Patient 3. **(D)** Immunoreactive macrophages (arrows) between several cerebral white matter lesions. Anti-tumor necrosis factor-α; original magnification: 600×. Patient 3. **(E)** Spheroids (arrows), a mineralized axon (arrowhead), and mineralized spheroid (s) in a cerebral white matter lesion. H and E; original magnification: 400×. Patient 1. **(F)** Central focus of mineralization as seen in Figure 1A surrounded by linear, pinwheel-like, losses of myelin and oligodendrocytes. Axons are still intact in such lesions. H and E; original magnification: 100×. Patient 1. **(G)** Two foci (arrows) of mineralization within cerebral white matter. H and E; original magnification: 100×. Patient 2. **(H)** Two foci of spheroids (arrows) in cerebral white matter. (Most of these spheroids are eosinophilic, but not argyrophilic with Bodian stain.) Anti-amyloid precursor protein; original magnification: 100×. Patient 3.

© 2007 American Association of Neuropathologists, Inc.

Downloaded from http://jnen.oxfordjournals.org/ by guest on June 7, 2016

Copyright © 2007 by the American Association of Neuropathologists, Inc. Unauthorized reproduction of this article is prohibited.

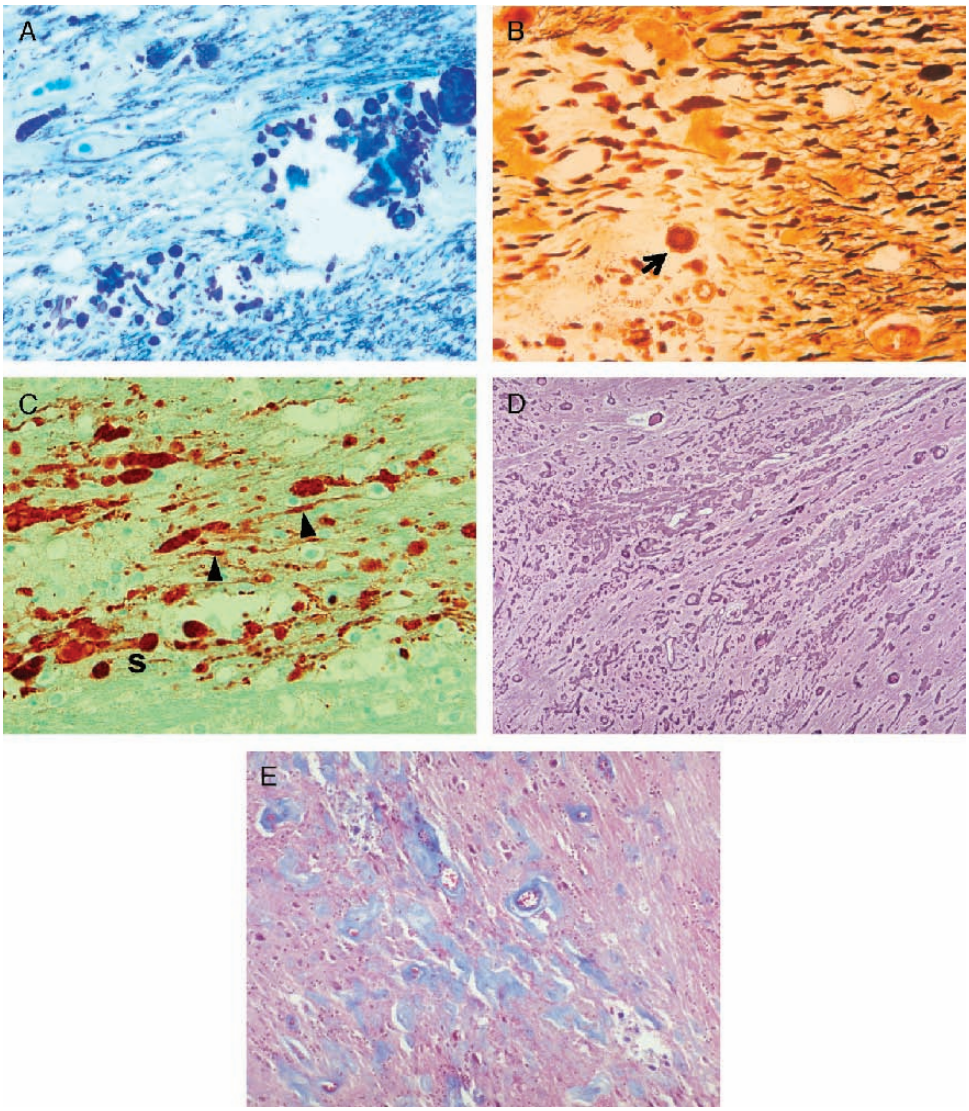

FIGURE 4. **(A)** Enlargement of a focus of decreased myelin staining in Figure 2B adjacent to a focus of mineralization (bottom and far right). Luxol fast blue; original magnification: 430×. Patient 1. **(B)** Loss of axons and axonal swellings in another pontine focus with enlargement of some surviving axons and a spheroid (arrow). Lester-King; original magnification: 430×. Patient 1. **(C)** Immunoreactive axons (arrowheads) and spheroids (s) in crossing fibers of the basis pontis. Anti-amyloid precursor protein; original magnification: 200×. Patient 3. **(D)** Another pontine lesion displaying increased microvascular reticulin staining. Reticulin; original magnification: 100×. Patient 1. **(E)** A comparable pontine lesion displaying microvascular fibrosis. Masson trichrome; original magnification: 430×. Patient 1.

lesions (Fig. 3F, G). Spheroids are most easily recognized in amyloid precursor protein-immunostained sections (Fig. 3H) and appear to be most numerous in our third patient.

The basis pontis in all cases shows the most severe and probably oldest lesions. The lesions display a loss of myelin sheaths and mineralization (Fig. 4A), as well as axonal loss and spheroids (Fig. 4B) that is again best seen in case 3 with the amyloid precursor protein immunostain (Fig. 4C). The chronicity of the pontine lesions is manifest as foci of a dense reticulin framework, most of it perivascular, (Fig. 4D) and both vascular and perivascular fibrosis (Fig. 4E).

The vascular abnormalities are also variable, but enlarged hyperchromatic endothelial cell nuclei are predominant (Fig. 5A). These are usually seen in small vessels of gray (i.e. capillaries) and white matter (i.e. venules and capillaries), but they are also rarely noted in small arteries/arterioles. These abnormal nuclei can be single and crescentic in shape (Fig. 5B) or are more vesicular and heaped up (Fig. 5C), or they appear to represent either multinucleated endothelial cells or circulating megakaryocytes (Fig. 5D). Their endothelial nature is supported by the occasional linear deposition of CD31 or CD34 immunoreactivity between the abnormal nuclei and vascular lumina (Fig. 5E). These endothelial cell abnormalities are found in otherwise normal gray (including cerebellar cortex) and white matter areas, but often near and rarely within the white

© 2007 American Association of Neuropathologists, Inc.

Downloaded from http://jnen.oxfordjournals.org/ by guest on June 7, 2016

Copyright © 2007 by the American Association of Neuropathologists, Inc. Unauthorized reproduction of this article is prohibited.

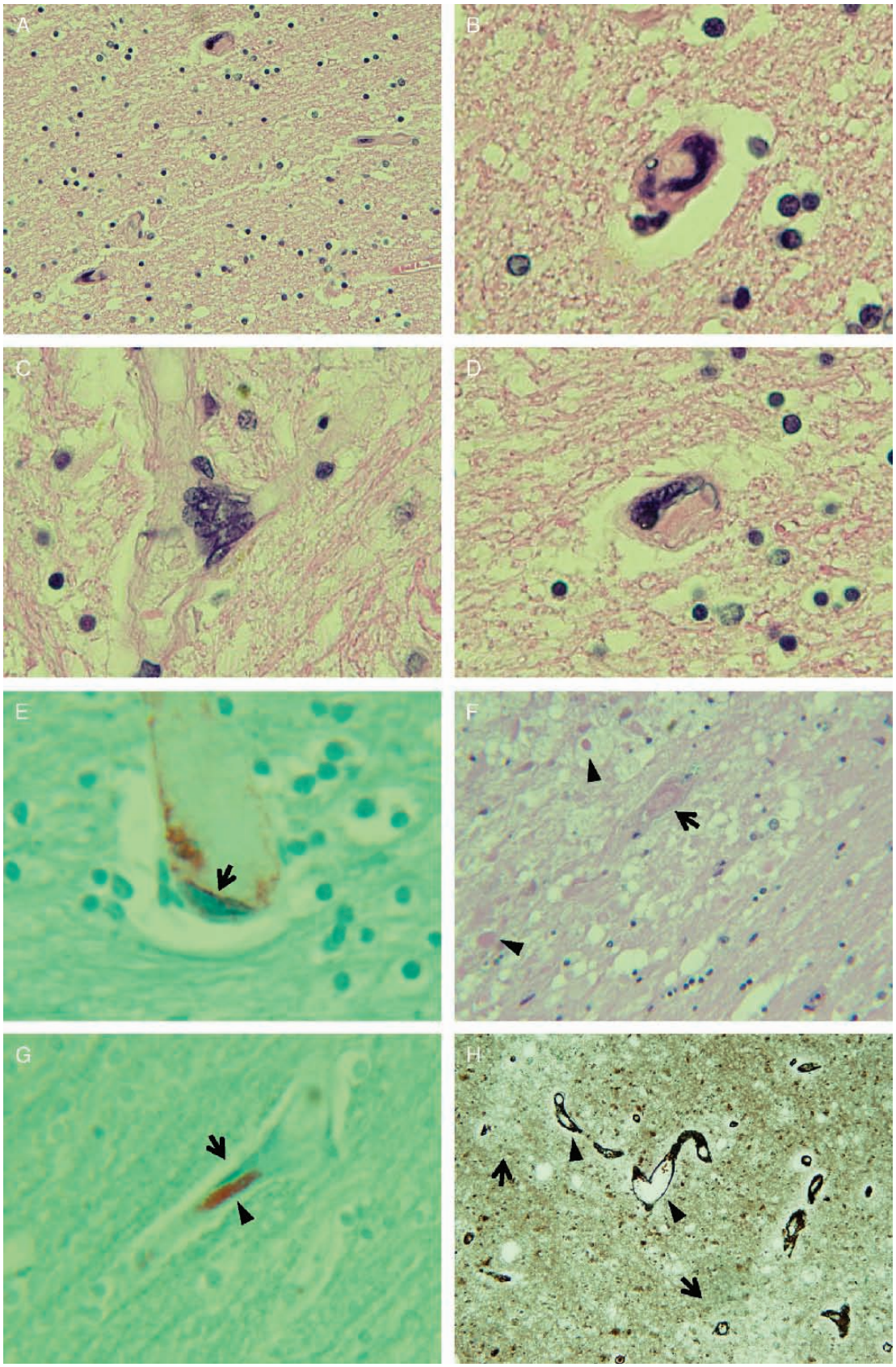

© 2007 American Association of Neuropathologists, Inc.

Downloaded from http://jnen.oxfordjournals.org/ by guest on June 7, 2016

Copyright © 2007 by the American Association of Neuropathologists, Inc. Unauthorized reproduction of this article is prohibited.

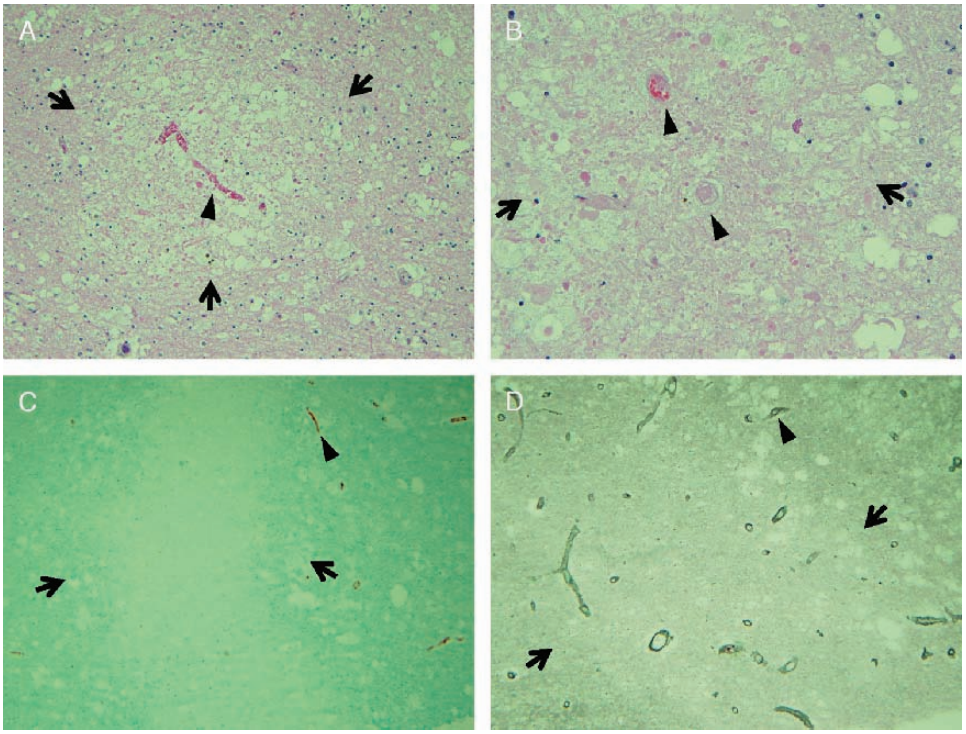

FIGURE 6. **(A)** Congested microvessel (arrowhead) at the center of a cerebral white matter lesion (within arrows). H and E; original magnification: 100×. Patient 3. **(B)** Two occluded and necrotic blood vessels (arrowheads) at the center of a necrotic cerebral white matter lesion (within arrows). H and E; original magnification: 200×. Patient 1. **(C)** Immunonegative lesion of cerebral white matter (within arrows); positive microvessel (arrowhead). Anti-CD31; original magnification: 50×. Patient 3. **(D)** Serial section of the same lesion of cerebral white matter (within arrows); numerous microvessels within and beyond (arrowhead) the lesion. Reticulin; original magnification: 50×. Patient 3.

matter lesions. They are also present in the upper cervical cord of patients 1 and 2 and in the optic nerves and pineal gland of patient 1. Groups of ectatic capillaries are found at the periphery of white matter lesions and in the cerebellar cortex. Some vessels in and near the white matter lesions may contain intraluminal eosinophilic material (Fig. 5F) that labels with antibodies to fibrin and platelets (factor VIII) (Fig. 5G). Capillaries or venules near or within the white matter lesions often are fibrotic, dilated, or mineralized (Fig. 5H). Some fibrotic microvessels, especially in advanced lesions, exhibit narrowed lumina. The vascular and axonal mineralizations reveal both iron and calcium (von Kossa- and alizarin red-positive) in some, but only 1 moiety in others, without any obvious predominance or sequence of deposition. Some white matter lesions are centered around small blood vessels (Fig. 6A, B), but, more commonly, the lesions are devoid of or deficient in small blood vessels, as if they have sustained a loss of endothelial cells in 1 or more microvessels. This is most apparent when one compares serial sections immunostained for CD31 or CD34 (both endothelial cell markers) (Fig. 6C) and reticulin stains (basal lamina and collagen markers) (Fig. 6D). None of the infection-related immunohistochemical stains or the PCR analysis for *Mycoplasma fermentans* revealed a culpable organism. The antibodies to herpes hominis virus-6 and *M. fermentans* weakly labeled the necrotic lesions in white matter. The abnormal endothelial cells could not be labeled with antibodies to p53 or Ki-67, the latter even at high pH.

No other significant neuropathologic findings were noted in patient 1 (even with von Kossa for calcium and iron, Lester-King, Masson trichrome, Luxol fast blue-cresyl violet, and reticulin stains) or in patient 3 (even with a

FIGURE 5. **(A)** Atypical endothelial nuclei (top middle, bottom left) in otherwise unremarkable cerebral white matter. H and E; original magnification: 200×. Patient 3. **(B)** Crescentic atypical endothelial nucleus. H and E; original magnification: 500× (oil). Patient 3. **(C)** Heaped-up, vesiculated endothelial nuclei in cerebral white matter. H and E; original magnification: 500× (oil). Patient 3. **(D)** Overlapping endothelial nuclei in cerebral white matter. H and E; original magnification: 500× (oil). Patient 3. **(E)** Linear immunoreactivity (arrow) between atypical endothelial nucleus (below) and lumen (above). Anti-CD34; original magnification: 500× (oil). Patient 1. **(F)** Myelin lesion in cerebral white matter with spheroids (arrowheads) and vacuolation containing an occluded, necrotic blood vessel (arrow). H and E; original magnification: 300×. Patient 3. **(G)** Atypical endothelial nucleus (arrow) adjacent to immunoreactive material within the lumen (arrowhead). Anti-factor VIII; original magnification: 300×. Patient 1. **(H)** Ectatic (arrowheads) and fibrotic blood vessels between 2 lesions of cerebral white matter displaying pallor and decreased numbers of nuclei (arrows). Reticulin; original magnification: 200×. Patient 1.

© 2007 American Association of Neuropathologists, Inc.

Downloaded from http://jnen.oxfordjournals.org/ by guest on June 7, 2016

Copyright © 2007 by the American Association of Neuropathologists, Inc. Unauthorized reproduction of this article is prohibited.

modified Bielschowsky, Gram, and Warthin-Starry stains and anti-tau, anti-β amyloid, anti-α synuclein, anti-CD68, and anti-CD3 immunostains). The orange discoloration of the globus pallidus of patient 1 was due to severe vascular mineralization (calcium and iron), and there was abundant iron-positive glial pigment in the brain of patient 2. Severe hypoxic damage in the form of marked neuronal loss and gliosis in the traditional gray matter sites was present, as well as some neuronal loss in substantia nigra without Lewy bodies.

Disease Controls

None of the cases of MNL in either immunocompromised or apparently immunocompetent patients, toxic

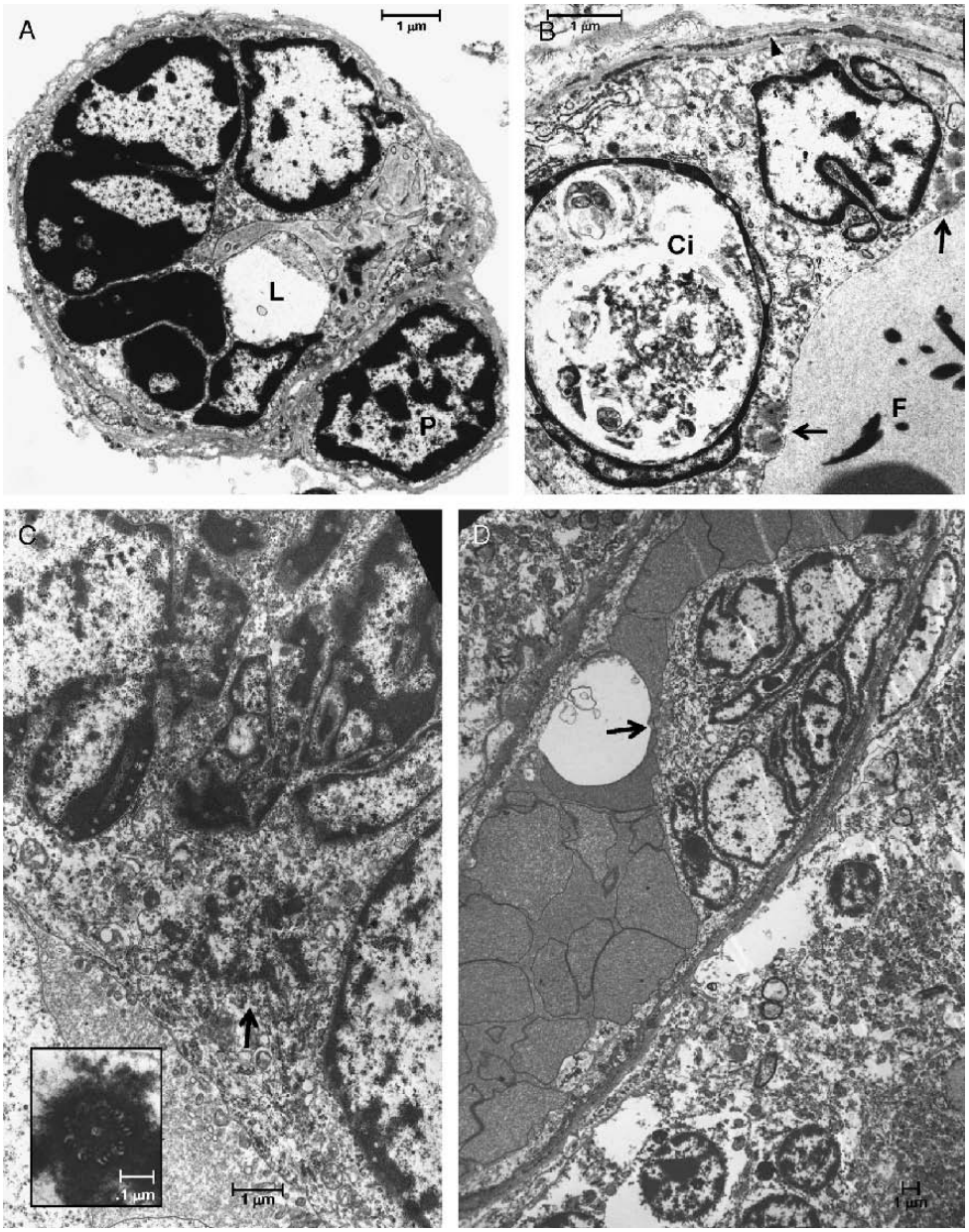

FIGURE 7. **(A)** Electron micrograph of cerebellar capillary with greatly constricted lumen (L) due to a large nuclear aggregate in lining endothelial cell. P, pericyte. Original magnification: 12,120×. Patient 1. **(B)** Transverse section of a cerebellar capillary with an endothelial cell expanded by 2 distorted nuclei. One contains a large invagination of degenerated cytoplasm (Ci). Mycoplasma-like particles are lined up along the cell membrane (arrows). Electron dense granular deposits are scattered within the split basal lamina (arrowhead). F, fibrin. Original magnification: 16,170×. Patient 1. **(C)** Group of centrioles (arrow) in the cytoplasm of a capillary endothelial cell with complex nuclear arrangement (top). Original magnification: 9,510×. Inset, Detail from another centriole cluster. Original magnification: 62,330×. Patient 1. **(D)** Multiple and/or distorted nuclei piled up in capillary endothelial cell (arrow) causing compromise of the lumen. Original magnification: 2,990×. Patient 1.

© 2007 American Association of Neuropathologists, Inc.

Downloaded from http://jnen.oxfordjournals.org/ by guest on June 7, 2016

Copyright © 2007 by the American Association of Neuropathologists, Inc. Unauthorized reproduction of this article is prohibited.

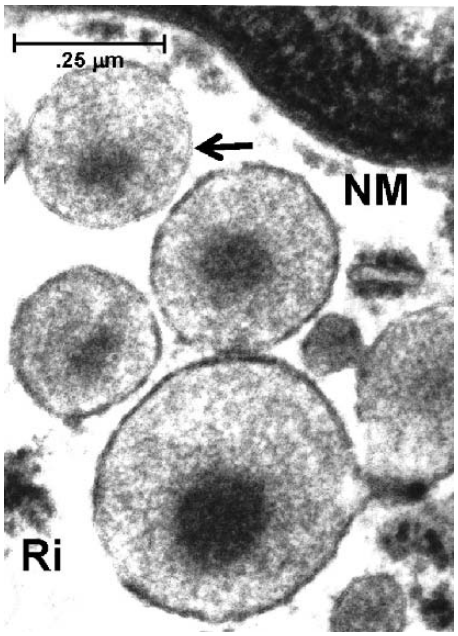

FIGURE 8. Cluster of mycoplasma-like particles (MLPs) in perinuclear cytoplasm of a capillary endothelial cell. The particles have a granular-fibrillar cytoplasm, nucleoids, and a trilaminar (arrow) cell membrane. The largest is approximately 420 nm in diameter. NM, nuclear membrane; Ri, ribosomes. Original magnification: 79,600×. Patient 1.

leukoencephalopathy, osmotic/central pontine myelinolysis, or bacterial sepsis exhibit the endothelial cell atypicalities of our 3 patients.

Ultrastructural Findings

Patient 1

Atypical Endothelial Nuclei

In greatly enlarged endothelial cells, bizarre nuclei, some of giant size, with intact nuclear envelopes are seen (Fig. 7A). The complex distortions of nuclear outlines are due to lobulations and cytoplasmic invaginations (Fig. 7B). Thin bridges of nuclear membrane can be seen to connect varying amounts of nuclear material. However, some of the nuclear aggregates show complete intervening stretches of cytoplasm, raising the question of multiple nuclei. This possibility is further supported by the presence of up to 10 centrioles in the cytoplasm of several of these cells (Fig. 7C). In some capillaries, the volume of the nuclear aggregates causes a compromise of their lumina (Fig. 7A, D). Several of the nuclei contain nuclear bodies of either fibrillar, granulofibrillar, or vesiculofibrillar appearance and of a mean size of 810 nm (range of 520 to 1100 nm).

Endothelial Cytoplasm and Cell Membrane

In endothelial cell cytoplasm features of focal degeneration are noted, such as partially or completely membrane-bound areas of rarefaction, aggregates of tubular profiles,

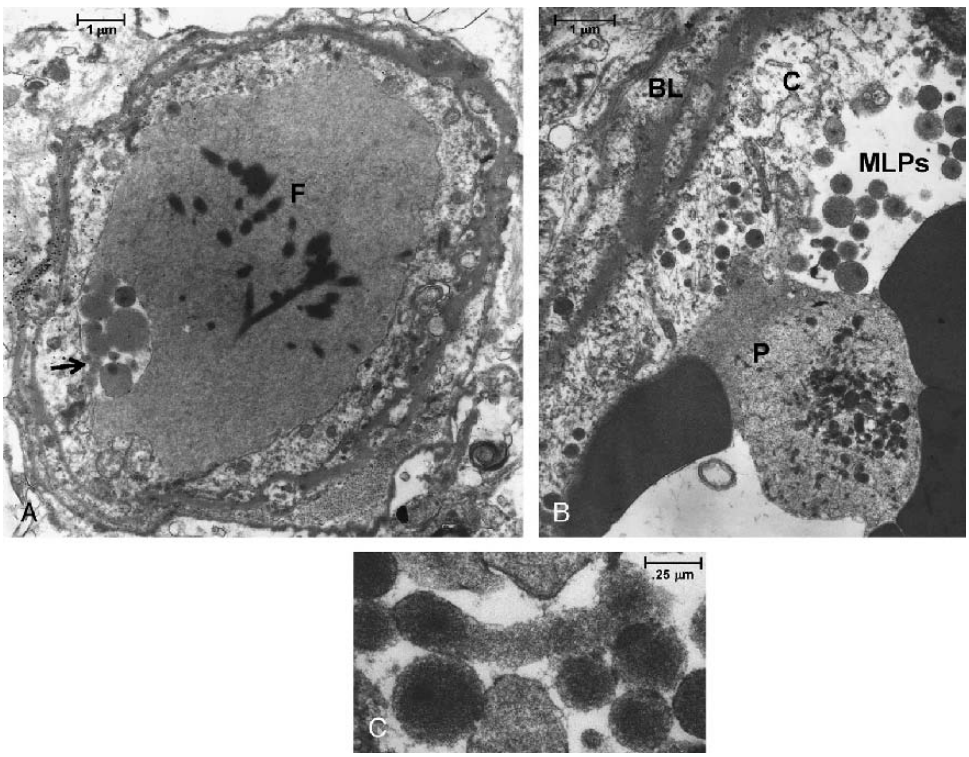

FIGURE 9. **(A)** Strands of fibrin (F) in capillary lumen together with a cluster of mycoplasma-like particles (MLPs) (arrow). Original magnification: 10,150×. Patient 1. **(B)** A platelet (P) adherent to disintegrating endothelial cytoplasm (C) next to clustered MLPs in lumen. Split basal lamina (BL). Original magnification: 12,440×. Patient 1. **(C)** An elongate MLP containing a nucleoid within a group of round intraluminal MLPs. Original magnification: 46,750×. Patient 1.

© 2007 American Association of Neuropathologists, Inc.

Downloaded from http://jnen.oxfordjournals.org/ by guest on June 7, 2016

Copyright © 2007 by the American Association of Neuropathologists, Inc. Unauthorized reproduction of this article is prohibited.

dispersed vesicles and granules, and myelin figures. Such changes are most prominent in the cytoplasmic invaginations into nuclei (Fig. 7B). Structural details of the cell cytoplasm as well as of the nuclei are incomplete owing to the postmortem sampling. However, there are definitely some unusual mycoplasma-like particles (MLPs) in different areas of the cell cytoplasm (Figs. 7B, 8), often close to the cell membrane. Sometimes aggregated in clusters, they are round, bordered by a trilaminar unit membrane (mean thickness 5.9 nm), and vary in size from 286 to 660 nm (mean 473 nm)

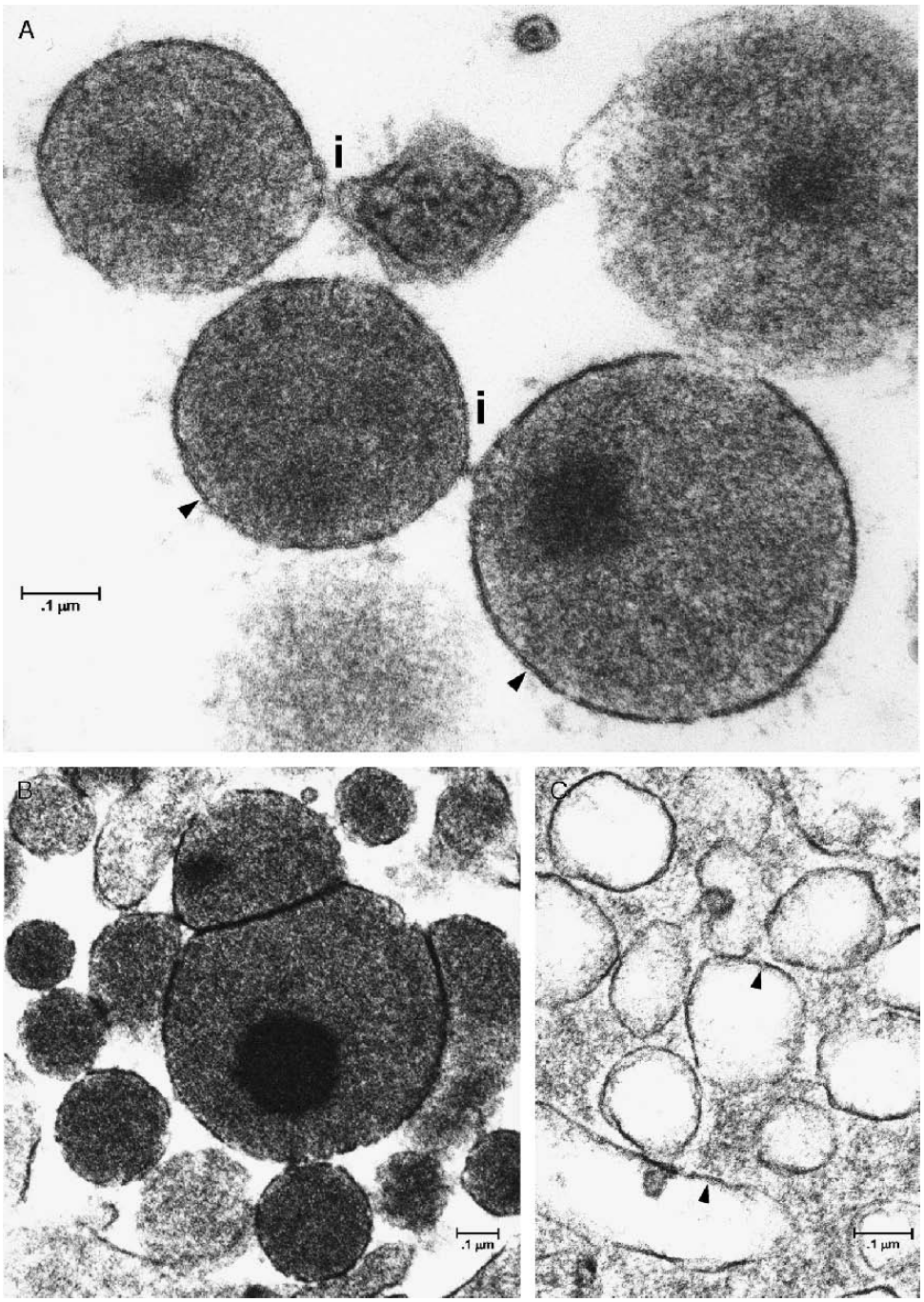

FIGURE 10. **(A)** Detail of an intraluminal cluster of mycoplasma-like particles (MLPs) with focal interconnections (i) of their trilaminar membranes (arrowheads). The largest is approximately 450 nm in diameter. Original magnification: 156,750×. Patient 1. **(B)** Cluster of intraluminal MLPs with an apparent budding process along the periphery of the largest one, measuring approximately 700 nm in diameter. Original magnification: 93,500×. Patient 1. **(C)** Collection of intraluminal empty MLPs of round shape, except for one partially seen elongate one (bottom), measuring approximately 140 nm in width. Trilaminar membranes are indicated by arrowheads. Original magnification: 137,500×. Patient 1.

© 2007 American Association of Neuropathologists, Inc.

Downloaded from http://jnen.oxfordjournals.org/ by guest on June 7, 2016

Copyright © 2007 by the American Association of Neuropathologists, Inc. Unauthorized reproduction of this article is prohibited.

(Fig. 8). Their matrix consists of granules and fibrils, with frequent electron-dense nucleoids. Rare images suggest a focal interruption of the unit membrane with spilling of some matrix contents, or focal absence of the unit membrane when the particle is in apposition to the cell membrane.

Capillary Lumina

Aside from blood cells, fibrin (Fig. 9A), and some cell debris, the capillary lumina contain MLPs, such as those seen in the endothelial cell cytoplasm. There is a wider range (300–1262 nm) and a greater mean size (781 nm) of these particles, many of which contain nucleoids. The largest particle clusters are noted at sites of endothelial cell plasma membrane defects. At 1 such site a platelet is found adherent to the disintegrating cell cytoplasm (Fig. 9B). Rare elongate forms with nucleoids are found in particle aggregates (Fig. 9C); the measurements of 2 are 122 nm × 767 nm and 157 nm × 1010 nm. The interconnectedness of round particles of differing sizes suggests a budding process (Fig. 10A, B). Within a few capillary lumina, collections of empty round particles (Fig. 10C), also with trilaminar membranes (6.7 nm) and with a size range from 138 to 522 nm (mean 330 nm) are observed. One empty elongate particle measures 224.5 nm × 1300 nm.

Endothelial Cell Junctions, Basal Lamina, and Abluminal Space

No definite abnormalities of intercellular tight junctions are noted. The basal lamina, approximately 250 nm wide, shows frequent focal duplications (Fig. 9B), and linear deposits of a finely granular electron-dense material occupy the spaces created in many of these splits (Fig. 7B). Within the abluminal space, occasional fragmented and curled membranes and myelin figures are seen.

Patient 2

Atypical Endothelial Nuclei

In a longitudinal section of a capillary 5 nuclei, or nuclear lobulations, are present within 1 endothelial cell, over a distance of 25 μm, causing a marked narrowing of the lumen. In a cross-sectioned vessel, 3 such nuclei, or nuclear lobulations, each with 1 nuclear body, are present in 1 endothelial cell.

Endothelial Cytoplasm and Cell Membrane

The cytoplasm of endothelial cells appears mostly disrupted, and no intact cell membranes are seen. In 1 cell 2 centrioles are present. No MLPs are seen.

Capillary Lumina

A considerable amount of unidentifiable granular and membranous cell debris is found in the lumina, in addition to red and white blood cells, platelets, and fibrin. The attachment of a platelet to damaged endothelial cell cytoplasm is noted (Fig. 11A). The lumen also contains singly scattered, or clustered MLPs ranging in size from 240 to 600 nm (mean of 420 nm), with a trilaminar surface membrane (mean of 6.3 nm), a fibrillogranular matrix, and a nucleoid in more than half. In well-preserved particles a trilaminar

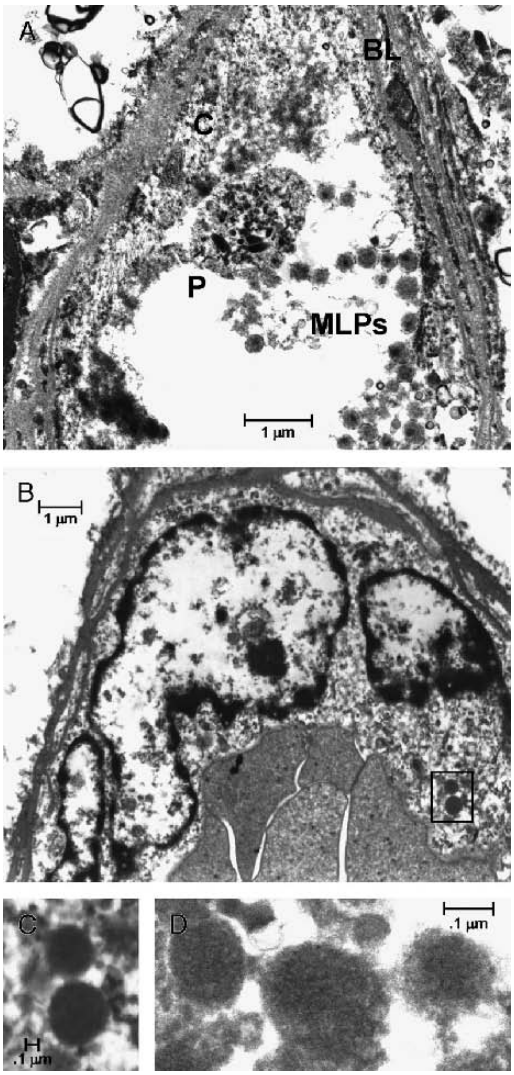

FIGURE 11. (A) Cerebellar capillary with a platelet (P) attached to disintegrating cytoplasm (C) and mycoplasma-like particles (MLPs) in lumen. BL, split basal lamina. Original magnification: 13,200×. Patient 2. **(B)** Cross-sectioned cerebral capillary with atypical nuclear arrangement of endothelial cell and 2 MLPs in cytoplasm (box). The largest is approximately 490 nm in diameter. Original magnification: 8,130×. Patient 3. **(C)** Detail of MLPs from **B**. Original magnification: 24,930×. Patient 3. **(D)** Small cluster of intraluminal MLPs with granular cytoplasm and without distinct cell membranes or nucleoids, the largest measuring approximately 250 nm in diameter. Original magnification: 95,000×. Patient 3.

surface membrane, measuring 6.3 nm, is seen. There are no empty particles. A few elongate particles of a granulofibrillar composition are noted together with the round ones, the largest measuring 220 nm × 800 nm. They have no distinct trilaminar membranes or nucleoids.

Endothelial Cell Junctions, Basal Lamina, and Abluminal Space

Tight junctions can be identified only rarely. The basal lamina, about 292 nm wide, shows duplication over most of

© 2007 American Association of Neuropathologists, Inc.

Downloaded from http://jnen.oxfordjournals.org/ by guest on June 7, 2016

Copyright © 2007 by the American Association of Neuropathologists, Inc. Unauthorized reproduction of this article is prohibited.

its course and electron-dense granules within the splits. A pericyte with a pyknotic nucleus is seen. Within the abluminal space no MLPs are identified.

Patient 3

Atypical Endothelial Nuclei

Multiple, or lobulated, enlarged endothelial nuclei are arranged in a crescent pattern along a capillary lumen (Fig. 11B).

Endothelial Cytoplasm and Cell Membrane

A small cluster of round MLPs is present in the cytoplasm of the same endothelial cell that has an intact plasma membrane (Fig. 11B, C). The largest particle measures 492 nm.

Capillary Lumina

Aside from erythrocytes and unidentifiable material, the lumina contain MLPs of granular appearance ranging in size from 136 to 550 nm (mean of 343 nm) (Fig. 11D). Adherence is noted among some round particles. Nucleoids are absent, and no distinct cell membranes can be identified. One elongate form is 157.5 × 322.2 nm in size.

Endothelial Cell Junctions, Basal Lamina, and Abluminal Space

Junctions are not identified. Duplication of the basal lamina is seen to a great extent. No MLPs are noticed in the abluminal space. Of note, no virions are seen in any of the tissues described above.

DISCUSSION

We have presented, to our knowledge, a new adult-onset progressive motor and cognitive syndrome that is due to multifocal white matter lesions in association with atypical, and perhaps multinucleated, endothelial cells and is restricted to the CNS. We also present ultrastructural data that strongly suggest that this disease is caused by the infection and destruction of endothelial cells in CNS microvessels by a mycoplasma-like microorganism.

The clinical syndrome in these 3 unrelated, apparently immunocompetent, adults consisted predominantly of weakness, ataxia, and spasticity of spinal and bulbar neuromuscular systems. The neuropathologic lesions responsible for this fatal disease are multifocal demyelinative to necrotizing lesions of white matter with varying degrees of mineralization at all levels of the neuraxis, but predominantly in cerebral white matter and basis pontis. These clinical and histologic features are similar to those of MNL, most commonly seen in immunosuppressed patients with the acquired immunodeficiency syndrome (AIDS) (9) or leukemia. There is a suggestion that the lesions of MNL might be caused by proinflammatory cytokines, such as TNF or IL-1 (11). As in MNL, the lesions in the basis pontis of our patients also appeared to be the largest and most mineralized (calcium and iron), suggesting that the pons was the earliest site of tissue injury. This postulate is supported by early bulbar signs or symptoms in patients 1 and 2. However, MNL differs from this new syndrome in at least 4 ways. First, the clinical course appears to be much shorter in MNL (i.e. weeks to months). Second, the patients with AIDS were immunocompromised and usually had concomitant infectious or neoplastic CNS processes. Third, none have demonstrated the endothelial cell atypicalities present in all 3 of our patients. Fourth, a mycoplasma-like organism within brain endothelial cells, to our knowledge, has never been reported in MNL (9). Similar to identical MNL-like lesions, particularly in pons, have also been seen in the clinical setting of intrathecal chemotherapy and CNS radiotherapy (late delayed radionecrosis) for the treatment of malignancies. This association might be a closer link to the presently described lesions in that vascular damage has been invoked as its most significant pathogenetic factor. Many of those neuropathologic lesions are identical to these reported here. However, again, none of those reports have described or demonstrated endothelial cell atypicalities (12, 13). In a single observation of disseminated CNS lesions after an unusually high-dose intravenous treatment with busulfan, a microangiopathy with endothelial cell proliferation, similar to that seen in delayed radiation necrosis, was reported in biopsy tissue (14). Likewise, none of our cases of osmotic/central pontine myelinolysis or any others reported in the literature (10, 15–23) have displayed such endothelial cell changes. Some of the perivascular lesions displaying loss of myelin staining, relative axonal preservation, loss of oligodendrocytes, spheroids, macrophages, and a mild astrocytic response have also been reported in the cerebral white matter of patients with pernicious anemia and cobalamin C deficiency (24, 25). The number of spheroids appeared to be fewer and macrophages greater in the latter 2 diseases; most importantly, the endothelial cell abnormalities of our patients were not present.

The white matter lesions appear to have a vascular origin, perhaps ischemic. In some lesions, the capillary or venular lumina appear to be narrowed by the atypical endothelial cells, whereas in others the vessel is necrotic and the lumen is often occluded by fibrin or platelets. In advanced lesions, because vessels are fibrotic, their lumina are constricted. In the cerebellar and cerebral cortices, the endothelial cell lesions are not associated with any parenchymal damage; but ectatic capillaries are often seen, and the lumen may be narrowed at the site of heaped up or multinucleated endothelial cells. Sometimes, platelets or fibrin are seen in apposition to such abnormal endothelial cells (Figs. 5G, 9B, 11A). Consequently, it appears that the abnormal endothelial cells compromise some microvascular lumina, produce stasis, and induce the activation of platelets and fibrin. When endothelial damage and death occur in this proposed scenario remains unclear. The cytokine TNF has been identified in and around the white matter lesions, primarily in macrophages, and may play a significant pathogenic role. TNF can increase the permeability of the blood-brain barrier (26). TNF is able to upregulate the prothrombotic plasminogen activator inhibitor-1 and tissue factor in endothelial cells; the latter in turn stimulates the transcription of TNF by endothelial cells and provides a positive feedback loop for TNF synthesis. TNF also depresses the expression of the anticoagulant thrombomodulin

© 2007 American Association of Neuropathologists, Inc.

Downloaded from http://jnen.oxfordjournals.org/ by guest on June 7, 2016

Copyright © 2007 by the American Association of Neuropathologists, Inc. Unauthorized reproduction of this article is prohibited.

in endothelial cells. Finally, TNF is able to induce an apoptotic death of endothelial cells. With the death of endothelial cells, platelets are exposed to basal lamina collagen and this promotes platelet adherence and aggregation (reviewed in Reference 27). Thus, one might postulate that the vascular damage and ensuing tissue destruction in our patients is largely cytokine-mediated, specifically by TNF, either produced locally or circulating. In view of our later discussion it may be noteworthy that 1) in Dengue fever, both the virus and TNF are critical for endothelial damage (28) and 2) that several *Mycoplasma* species can stimulate the production of TNF in cultured rat astrocytes (*M. fermentans* and *Mycoplasma capricolum*) (29) and human peripheral blood mononuclear cells (*M. pneumoniae, Mycoplasma hyorhinis, Mycoplasma arginini, Mycoplasma salivarium, Mycoplasma orale,* and *Mycoplasma gallisepticum*) (30). The reason that the vascular abnormalities are associated with damage to white matter (i.e. myelin, oligodendrocytes, and axons) but not to gray matter remains problematic. Perhaps some circulating white matter toxin crosses an already defective blood-brain barrier. Alternatively, perhaps the higher concentration of microglia, the major source of TNF in white matter (versus gray matter), results in a selective vulnerability of the former. It is again noteworthy that the highest concentration of microglia in the normal adult CNS is in the pons (31).

Atypical, perhaps multinucleated, endothelial cells of the microvasculature are the hallmark of this new disease. A variety of endothelial nuclear changes have been reported as the result of direct invasion by DNA or RNA viruses of human or animal origin. These studies were carried out in CNS or other tissues, or in endothelial cell cultures. Cytomegalovirus infection results in the formation of Cowdry-A type nuclear inclusions (32). Intranuclear inclusions without halos are present in enlarged hyperchromatic nuclei after infection with either human BK-related polyoma virus (33) or with murine Papova virus K (34). Nuclear enlargement and hyperplasia is associated with human immunodeficiency virus infection (35). Formation of polynuclear giant cells is the result of infection with either Marburg virus (36) or Nipah virus (37). Multinucleated giant cells and syncytia are observed in cultures infected with human T-lymphotropic virus type 1 (38). Endothelial cell pathology after infection with murine leukemia virus TR1.3 includes formation of syncytia (6), with the ultrastructural demonstration of intracytoplasmic clefts.

The motivation for our ultrastructural studies came from some of the above literature. However, the search for virus particles remained negative. Instead, particles exceeding viral dimensions, with rare ones only in the vaccinia range, were detected in endothelial cytoplasm and capillary lumina, but never in endothelial cell nuclei. From descriptions and depictions in the literature (see below) they are best interpreted as *Mycoplasma* species, class Mollicutes, the smallest bacterial organisms, with a DNA genome and lacking a cell wall.

Mycoplasma organisms are known for variability in size and variations in shape. In comparing the sizes of our MLPs with the dimensions of proven organisms presented in the literature, one has to consider variations in sampling (from tissues or cultures) and in processing techniques, in addition to the influence of a given *Mycoplasma* species and the phase of their cell development. The preferential size of 400 to 600 nm for round-shaped particles in our studies, with a range of 136 to 1262 nm, is compatible with sizes published for *Mycoplasmas*: 140 to 280 nm for *M. fermentans incognitus* (39), 140 to 840 nm for *Ureaplasma* (40), and 200 to 800 nm for *Mycoplasma*, species not specified (41). Elongate forms of MLPs were seen infrequently in our cases 1 and 2. Described as "filamentous," and occasionally with branching, they have been shown for *Mycoplasma laidlawii* and *M. ovale* and *Mycoplasma hominis* (40), for *Mycoplasma incognitus* (42) and for *M. gallisepticum* (43), among others. Elongate flask-shaped forms were depicted for *Mycoplasma pirum* and *Mycoplasma penetrans* (44). Rare intraluminal aggregates of empty, round, or elongate MLPs were found in our patient 1. Such electron microscopy images have been observed at certain levels of cultures of *Mycoplasma canis* (45) and of *M. orale* (46), in cultures of *M. laidlawii* after exposure to antiserum and complement (47), and in a fixed specimen of *Ureaplasma* cells (40). Whether immune lysis, autolysis, or perhaps changes in osmolality had any influence on the loss of cytoplasm of these MLPs in our material is open to speculation. In our studies, no tip-like structures on the cell surface, such as those observed for *M. pneumoniae* or *M. penetrans* (48) and related to cell adhesion and invasion have been observed. The basic ultrastructural components of MLPs included a trilaminar surface membrane from 5.9 to 6.7 nm in width and a matrix composed of granules and fibrils with focal condensation of the latter into a nucleoid. A trilaminar cell membrane is an identifying characteristic for *Mycoplasma* species, with measurements from 7.5 to 10 nm (49). The granules in the cytoplasm represent ribosomes and the filaments represent DNA strands (49). With regard to the nucleoids, only 1 such image was found in the literature, pertaining to *M. gallisepticum* (43). In contrast, other observers (40, 45) have identified nuclear regions as central areas with a few delicate filaments only in *Mycoplasma pulmonalis* and *M. hominis*. Such areas were never noticed in our material. The nucleoids seen frequently in our material are probably not the result of preparatory techniques. Could they be characteristic of a new *Mycoplasma* species? The presence of smaller-sized MLPs connected to the surface of larger ones or grouped in clusters around them, suggests a budding process. Such a mode of multiplication has been reported in the literature for *Mycoplasma* species (41) in addition to binary fission. It may be noteworthy that few MLPs could be identified in patient 3, who had been treated vigorously with a host of antibiotics, including a macrolide, a tetracycline, and a fluoroquinolone, all of which are used to treat *Mycoplasma* infections.

Some of our ultrastructural observations suggest pathogenic features of the putative organisms. A cytopathic-cytolytic activity for endothelial cells seems apparent from the presence of MLPs along the luminal surfaces of disintegrating cells with the adherence of platelets at the site of injury and with various cell debris present in the lumina

© 2007 American Association of Neuropathologists, Inc.

Downloaded from http://jnen.oxfordjournals.org/ by guest on June 7, 2016

Copyright © 2007 by the American Association of Neuropathologists, Inc. Unauthorized reproduction of this article is prohibited.

together with numerous MLPs. Duplicated basal laminae, most likely the result of chronic cell injury (50), were frequently seen.

Mycoplasma organisms are parasitic bacteria, and their relationship with host cells has been detailed by Rottem (51) and reviewed by Baseman and Tully (52). Pertinent data have been obtained exclusively from in vitro experiments with mammalian cells. The small genome size of *Mycoplasma* organisms creates the need for metabolic products from their host cells to supplement their requirements. The attachment to host cells is based on *Mycoplasma* adhesins and host cell receptors. Attachment alone, without invasion, also may lead to cytopathic effects, because the competition for nutrients can cause depletion in the host cell and thus interfere with its maintenance and function. Additional damage can be caused by the secretion of *Mycoplasma* enzymes, such as ATPase and proteases and by oxidative stress. The entrance of *Mycoplasma* organisms into host cells may follow changes in cell surface proteins. The sequence of parasite attachment, cell invasion, and cell death has been documented by electron microscopy for human umbilical cord endothelial cells exposed to *M. penetrans* (48).

Immunohistochemistry of white matter lesions in our patients revealed the presence of TNF, primarily in macrophages. The capability of *Mycoplasma* organisms to induce production of TNF in macrophages has been well documented. Gallily et al (53) reported that *M. orale*-induced TNF in macrophages caused, or at least participated in, the lysis of cultured fibrosarcoma cells. Four other *Mycoplasma* species showed a variable degree of efficiency. The authors even suggested the use of *M. orale* for the treatment of human cancer. Mühlradt and Schade (54) demonstrated the production of TNF by rodent macrophages after exposure to a cell product of *M. fermentans*, and Kaufmann et al (55) observed TNF release from human monocytes after exposure to a lipoprotein derived from *M. fermentans* cell membranes.

Is there any evidence in favor of *Mycoplasma* organisms relating to and invading human cerebral capillary endothelial cells? In 1989, Lo et al (56) published ultrastructural studies of autopsy brains of patients with AIDS. In a histologically unremarkable brainstem sample that, however, had been highly positive antigenically for *M. incognitus*, they found typical *Mycoplasma*-like particles within an endothelial cell, seemingly of a capillary.

Our ultrastructural studies devoted to the analysis of the atypical nuclei revealed their presence within giant cells with intact cell membranes and with MLPs in the cytoplasm of some. There were no intracytoplasmic clefts suggestive of syncytial formation. No cell membranes separated the nuclear material. Multiple centrioles were noted in several cells, but there were no spindle tubules. In the absence of serial sections, we could not resolve whether nuclear multiplicity existed or whether the giant nuclear aggregates derived solely from bizarrely configured single nuclei. Nuclear enlargement and distortion from infoldings has been observed by electron microscopy in canine brain endothelial cells in delayed radiation necrosis (57), and complex ultrastructural distortions of cerebellar capillary endothelial cells were noted in a child after a high-dose treatment with busulfan (Reference 14 and Margaret Grunnett, MD, personal communication, 1991). For both x-irradiation and exposure to alkylating agents, the resultant chromosomal damage is well known. Nuclear distortions also occur in tumor cells, and cytoplasmic invaginations are common in meningiomas and glioblastomas that show an abnormal configuration of chromosomes, or loss, respectively. Some of the nuclei we observed (Fig. 7C) are particularly reminiscent of the "cerebriform" nuclei of Sézary cells of cutaneous T-cell lymphoma.

We assume that the nuclear atypia in our patients was based on chromosomal abnormalities with resultant aneuploidy. The negative immunolabeling for Ki-67, indicating a lack of proliferative potential, is supported by our electron microscopy findings. Could the nuclear abnormalities be a pathogenic feature of the putative mycoplasma? Nucleases are among the enzymes secreted by *Mycoplasma* organisms (52). In 1965, Paton et al (58) conducted the first study on chromosomes in normal cells exposed to a *Mycoplasma* species. They found that *M. orale* induced structural abnormalities of chromosomes, breaks, and polyploidy in WI-38 human embryonic lung cultures. Stanbridge et al in 1960 (59) observed frequent chromosomal breaks and translocations and pulverization in WI-38 cells after exposure to 5 *Mycoplasma* species; *M. orale* only induced abnormal, large nuclei with a spotted chromatin. The oncogenic effect, mostly in vitro, of *Mycoplasma* species has been the subject of study by Lo and his collaborators for more than a decade. Persistent infection of cultured mouse fibroblast cells with *M. fermentans* or *M. penetrans* led to irreversible transformation and the ability for sarcoma induction after subcutaneous inoculation in mice. Chromosomal translocations were prominent in transformed cells and tumor cells (60). Reciprocal translocations were detected subsequently in cultured human peripheral blood monocytes immortalized after prolonged exposure to *M. fermentans* (61).

Future progress in solving the many questions posed by this new disease will require the alertness and collaboration of neurologists, bacteriologists, and neuropathologists. Because of the seeming rarity of the disease and the difficulty in culturing *Mycoplasma* species, it may take many years of work, and some luck, to know the nature of the MLPs. For the same reasons, it took 7 years to achieve culture of JC virus in progressive multifocal leukoencephalopathy after the discovery of the Papova-like virions by electron microscopy (62, 63).

ACKNOWLEDGMENTS

We thank Drs. Gary K. Ludwig, Osmar A. Pinella, Richard Hessler, and Greer Falls for these referrals. We appreciate the immunohistochemical expertise of Patricia Bourne and Frances Vito, the excellent technical assistance in electron microscopy of Joan Sempf and Steve Coleman, and the usual outstanding secretarial support of Tina Blazey and Linda Crandall. Finally, we are grateful to the daughter of patient 3 for providing the MRIs of her father for expert review by Professor Marjo van der Knaap of the Free University Medical Center in Amsterdam, The Netherlands.

© 2007 American Association of Neuropathologists, Inc.

Downloaded from http://jnen.oxfordjournals.org/ by guest on June 7, 2016

Copyright © 2007 by the American Association of Neuropathologists, Inc. Unauthorized reproduction of this article is prohibited.

REFERENCES

1. Tsiodras S, Kelesidis I, Kelesidis T, et al. Central nervous system manifestations of *Mycoplasma pneumoniae* infections. J Infect 2005;51: 343–54
2. Behan PO, Feldman RG, Segerra JM, et al. Neurological aspects of mycoplasmal infection. Acta Neurol Scand 1986;74:314–22
3. Tsiodras S, Kelesidis T, Kelesidis I, et al. *Mycoplasma pneumoniae*-associated myelitis: A comprehensive review. Eur J Neurol 2006;13: 112–24
4. Narita M, Itakura O, Matsuzono Y, et al. Analysis of mycoplasmal central nervous system involvement by polymerase chain reaction. Pediatr Infect Dis J 1995;14:236–37
5. Sočan M, Ravnik I, Benčina D, et al. Neurological symptoms in patients whose cerebrospinal fluid is culture-and/or polymerase chain reaction-positive for *Mycoplasma pneumoniae*. Clin Infect Dis 2001;32:e31–e35
6. Park BH, Lavi E, Stieber A, et al. Pathogenesis of cerebral infarction and hemorrhage induced by a murine leukemia virus. Lab Invest 1994; 71:78–85
7. Wang RY-H, Lo S-C. PCR detection of *Myoplasma fermentans* infection in blood in urine. In: Persing D, Smith TF, Tenover FC, White TJ, eds. *Diagnostic Molecular Microbiology, Principles and Applications.* Rochester, MN: American Society for Microbiology, Mayo Foundation, 1993:511–16
8. di Sant'Agnese PA, de Mesy-Jensen KL. Diagnostic electron microscopy on reembedded ("popped off") areas of large Spurr epoxy sections. Ultrastruct Pathol 1984;6:247–53
9. Anders KH, Becker PS, Holden JK, et al. Multifocal necrotizing leukoencephalopathy with pontine predilection in immunosuppressed patients: A clinicopathologic review of 16 cases. Hum Pathol 1993;24: 897–904
10. Adams RD, Victor M, Mancall EL. Central pontine myelinolysis: A hitherto undescribed disease occurring in alcoholic and malnourished patients. Arch Neurol 1959;81:154–72
11. Gray F, Bélec L, Chrétien F, et al. Acute, relapsing brain oedema with diffuse blood-brain barrier alteration and axonal damage in the acquired immunodeficiency syndrome. Neuropathol Appl Neurobiol 1998;24: 209–16
12. Pennybacker J, Russell DR. Necrosis of the brain due to radiation therapy: Clinical and pathological observations. J Neurol Neurosurg Psychiatry 1948;11:183–98
13. Bruner JM, Tien RD, Thorstad WL. Structural changes produced by intracranial tumors and various forms of antineoplastic therapy. In: Bigner DD, McLendon RE, Bruner JM, eds. *Russell and Rubinstein's Pathology of Tumors of the Nervous System.* London: Arnold, 1998:2: 451–91
14. Zalneraitis EL, Grunnett ML, Quinn JJ, et al. Isolated central nervous system angiopathy associated with busulfan (Abstract). Ann Neurol 1989;26:478
15. Goebel HH, Herman-Ben Zur P. Central pontine myelinolysis: A clinical and pathological study of 10 cases. Brain 1972;95:495–504
16. Wright DG, Laureno R, Victor M. Pontine and extrapontine myelinolysis. Brain 1979;102:361–85
17. Endo Y, Oda M, Hara M. Central pontine myelinolysis: A study of 37 cases in 1,000 consecutive autopsies. Acta Neuropathol 1981;53: 145–53
18. Boon AP, Potter AE. Extensive extrapontine and central pontine myelinolysis associated with correction of profound hyponatraemia. Neuropathol Appl Neurobiol 1987;13:1–9
19. Riggs JE, Schochet SS Jr. Osmotic stress, osmotic myelinolysis, and oligodendrocyte topography. Arch Pathol Lab Med 1989;113:1386–88
20. Gocht A, Colmant HJ. Central pontine and extrapontine myelinolysis: A report of 58 cases. Clin Neuropathol 1987;6:262–70
21. Medana IM, Esiri MM. Axonal damage: A key predictor of outcome in human CNS diseases. Brain 2003;126:515–30
22. Ghosh N, DeLuca GC, Esiri MM. Evidence of axonal damage in human acute demyelinating diseases. J Neurol Sci 2004;222:29–34
23. Kleinschmidt-DeMasters BK, Rojiani AM, Filley CM. Central and extrapontine myelinolysis: Then…and now. J Neuropathol Exp Neurol 2006;65:1–11
24. Adams RD, Kubik CS. Subacute degeneration of the brain in pernicious anemia. N Engl J Med 1944;231:1–9
25. Powers JM, Rosenblatt DS, Schmidt RE, et al. Neurological and neuropathologic heterogeneity in two brothers with cobalamin C deficiency. Ann Neurol 2001;49:396–400
26. de Vries HE, Blom-Rousemalen MCM, van Oosten M, et al. The influence of cytokines on the integrity of the blood-brain barrier in vitro. J Neuroimmunol 1996;64:37–43
27. Marder VJ, Feinstein DI, Colman RW, et al. Consumptive thrombohemorrhagic disorders. In: Colman RW, Clowes AW, Goldhaber SZ, Marder VJ, George JN, eds. *Hemostasis and Thrombosis: Basic Principles and Clinical Practice.* Philadelphia: Lippincott Williams & Wilkins, 2006:1571–72
28. Chen HC, Hofman FM, Kung JT, et al. Both virus and TNF-α are critical in endothelium damage in a dengue virus-induced hemorrhage mouse model. J Virol 2007;81:5518–26
29. Brenner T, Yamin A, Abramsky O, et al. Stimulation of tumor necrosis factor-α production by mycoplasmas and inhibition by dexamethasone in cultured astrocytes. Brain Res 1993;608:273–79
30. Kita M, Ohmoto Y, Hirai Y, et al. Induction of cytokines in human peripheral blood mononuclear cells by mycoplasmas. Microbiol Immunol 1992;36:507–16
31. Mittelbronn M, Dietz K, Schluesener HJ, et al. Local distribution of microglia in the normal adult human central nervous system differs by up to one order of magnitude. Acta Neuropathol 2001;101:249–55
32. Case Records of the Massachusetts General Hospital (Case 17-1996). N Engl J Med 1996;334:1461–67
33. Petrogiannis-Haliotis T, Sakoulas G, Kirby J, et al. BK-related polyomavirus vasculopathy in a renal-transplant recipient. N Engl J Med 2001;345:1250–55
34. Ikeda K, Dörries K, ter Meulen V, et al. Morphological and immunohistochemical studies of the central nervous system involvement in papovavirus K infection in mice. Acta Neuropathol 1988;77:175–81
35. Smith TW, DeGirolami V, Hénin D, et al. Human immunodeficiency virus (HIV) leukoencephalopathy and the microcirculation. J Neuropathol Exp Neurol 1990;49:357–70
36. Oehlert W. The morphological picture in livers, spleens and lymph nodes of monkeys and guinea pigs after infection with the "Vervet Agent." In: Martini GA, Siegert R. *Marburg Virus Disease.* New York: Springer Verlag, 1971:150
37. Bellini WJ, Harcourt BH, Bowden N, et al. Nipah virus: An emergent paramyxovirus causing severe encephalitis in humans. J Neurovirol 2005;11:481–87
38. Ho DD, Rota TR, Hirsch MS. Infection of human endothelial cells by human T-lymphotropic virus type 1. Proc Natl Acad Sci USA 1984;81: 7588–90
39. Lo SC, Wear DJ, Shih WK, et al. Fatal systemic infections of nonhuman primates by Mycoplasma fermentans (incognitus stain). Clin Infect Dis 1993;17:S283–88
40. Holt SC. Bacteria. In: Johannessen JV, ed. *Electron Microscopy in Human Medicine.* New York: McGraw-Hill, 1980;3:91–278
41. Willett HP. Mycoplasma. In: Joklik WK, Willett H, Amos DB, Wilfert CM. *Zinsser Microbiology.* Norwalk, CT: Appleton & Lange, 1992:730
42. Lo SC, Shih JWK, Newton PB III, et al. Virus-like infectious agent (VLIA) is a novel pathogenic mycoplasma: *Mycoplasma incognitus*. Am J Trop Med Hyg 1989;41:586–600
43. Zucker-Franklin D, Davidson M, Thomas L. The interaction of mycoplasmas with mammalian cells. I HeLa cells, neutrophils, and eosinophils. J Exp Med 1966;124:521–32
44. Blanchard A, Montagnier L. AIDS-associated mycoplasmas. Annu Rev Microbiol 1998;48:687–712
45. Domermuth CH, Nielsen MH, Freundt EA, et al. Ultrastructure of *Mycoplasma* species. J Bacteriol 1964;88:727–44
46. Nakamura M, Kawaguchi M. Ultrastructure of *Mycoplasma orale* serotype 1 in agar growth. J Gen Microbiol 1972;70:305–15
47. Brunner H, Dörner I, Schiefer HG, et al. Lysis of *Acholeplasma laidlawii* by antibodies and complement. Infect Immunol 1976;13: 1671–77
48. Lo SC, Hayes MM, Kotani H, et al. Adhesion onto and invasion into mammalian cells by *Mycoplasma penetrans*: A newly isolated *Mycoplasma* from patients with AIDS. Mod Pathol 1993;6:276–80
49. Freundt EA, Vinther O. Mycoplasmas. In: Johannessen JV, ed. *Electron Microscopy in Human Medicine.* New York: McGraw-Hill, 1980: 369–87

© 2007 American Association of Neuropathologists, Inc.

Downloaded from http://jnen.oxfordjournals.org/ by guest on June 7, 2016

Copyright © 2007 by the American Association of Neuropathologists, Inc. Unauthorized reproduction of this article is prohibited.

50. No author. Lesions of extracellular matrix and vascular tissue. In: Cheville NF. *Ultrastructural Pathology: An Introduction to Interpretation.* Ames: Iowa State University Press, 1994:289
51. Rottem S. Invasion of Mycoplasmas into and fusion with host cells. In: Razin S, Herrmann R, eds. *Molecular Biology and Pathogenicity of Mycoplasmas.* New York: Kluwer Academic/Plenum Publishers, 2002: 391–401
52. Baseman JB, Tully JG. Mycoplasmas: Sophisticated, reemerging and burdened by their notoriety. Emerg Infect Dis 1997;3:21–32
53. Gallily R, Sher T, Ben-Av P, et al. Tumor necrosis factor as a mediator of *Mycoplasma orale*-induced tumor cell lysis by macrophages. Cell Immunol 1989;121:146–53
54. Mühlradt PF, Schade U. MDHM, a macrophage-stimulatory product of *Mycoplasma fermentans*, leads to in vitro interleukin-1 (IL-1), IL-6, tumor necrosis factor, and prostaglandin production and is pyrogenic in rabbits. Infect Immunol 1991;59:3969–74
55. Kaufmann A, Mühlradt PF, Gemsa D, et al. Induction of cytokines and chemokines in human monocytes by *Mycoplasma fermentans*-derived lipoprotein MALP-2. Infect Immunol 1999;67:6303–8
56. Lo SC, Dawson MS, Wong DM, et al. Identification of *Mycoplasma incognitus* infection in patients with AIDS: An immunohistochemical, in situ hybridization and ultrastructural study. Am J Trop Med Hyg 1989;41:601–16
57. Yamaguchi N, Yamashima T, Yamashita J. A histological and flow cytometric study of dog brain endothelial cell injuries in delayed radiation necrosis. J Neurosurg 1991;74:625–32
58. Paton GR, Jacobs JP, Perkins FT. Chromosome changes in human diploid-cell cultures infected with *Mycoplasma*. Nature 1965;207:43–45
59. Stanbridge E, Önen M, Perkins FT, et al. Karyological and morphological characteristics of human diploid cell strain WI-38 infected with *Mycoplasmas*. Exp Cell Res 1969;57:397–410
60. Tsai S, Wear DJ, Shih JWK, Lo SC. Mycoplasmas and oncogenesis: Persistent infection and multistage malignant transformation. Proc Natl Acad Sci USA 1995;92:10197–201
61. Zhang S, Tsai S, Wu TT, et al. *Mycoplasma fermentans* infection promotes immortalization of human peripheral blood mononuclear cells in culture. Blood 2004;104:4252–59
62. ZuRhein GM, Chou SM. Particles resembling papova viruses in human cerebral demyelinating disease. Science 1965;148:1477–79
63. Padgett BL, Walker DL, ZuRhein GM, et al. Cultivation of papova-like virus from human brain with progressive multifocal leukoencephalopathy. Lancet 1971;1:1257–60

Downloaded from http://jnen.oxfordjournals.org/ by guest on June 7, 2016

© 2007 American Association of Neuropathologists, Inc.

Copyright © 2007 by the American Association of Neuropathologists, Inc. Unauthorized reproduction of this article is prohibited.